Tyrosine 64 of Cytochrome c_{553} Is Required for Electron Exchange with Formate Dehydrogenase in *Desulfovibrio vulgaris* Hildenborough

Corinne Sebban-Kreuzer,[‡] Martin Blackledge,[§] Alain Dolla,[‡] Dominique Marion,[§] and Françoise Guerlesquin*[,‡]

Unité de Bioénergétique et Ingénierie des Protéines, IBSM-CNRS, 13402 Marseille, France, and Institut de Biologie Structurale Jean-Pierre Ebel, CEA-CNRS, 38027 Grenoble, France

Received January 20, 1998; Revised Manuscript Received March 31, 1998

ABSTRACT: Replacement of tyrosine 64 by alanine in cytochrome c_{553} from *Desulfovibrio vulgaris* Hildenborough prevents electron transfer with the formate dehydrogenase. Biophysical and biochemical studies show that the protein is correctly folded and that the oxidoreduction potential is not modified. The solution structure of the mutant cytochrome determined by two-dimensional (2D) NMR clearly establishes that the overall fold of the molecule is nearly identical to that of the wild-type cytochrome. The electrostatic surface charge distributions for the wild-type and mutant cytochrome are similar, suggesting that the interaction site of the physiological partners is not modified by the mutation. The lack of the aromatic ring induces slight destabilization of the hydrophobic core of the molecule and modifications of the hydrogen bond at position 64, as well as conformational disorder of the side chain of K63. The loss of the hydrogen bond from tyrosine 64 and the increase of the solvent exposure of the heme are probably responsible of the loss of electron transfer between formate dehydrogenase and cytochrome c_{553}.

The mechanism of electron exchange in oxidoreduction complexes is a current matter of considerable interest in structural biology and genetics. The physical basis of long-range electron transfer in metalloproteins has been described by many groups (*1*). Two principal mechanisms of electron exchange have been proposed, which follow through-bond or through-space pathways (*2*). Numerous crystallographic structures of membrane complexes such as cytochrome oxidase (*3*) and the reaction center (*4*) have been solved. However, conclusive evidence has not yet been provided regarding the relative importance of the polypeptide chain or noncovalent interactions for the transfer of an electron from donor to acceptor within these complexes.

Site-directed mutagenesis is a useful tool for probing this kind of information, and cytochrome *c* provides an ideal focus for investigating factors that influence the rate of electron transfer within a complex. While the biochemical and physical characteristics of this family of proteins have been studied in detail (*5*), little information about electron transfer in complexes involving cytochromes *c* is available. It has nevertheless been established that the electron transfer reaction is driven by electrostatic interactions involving the highly conserved lysine residues of cytochromes *c* (*5*, *6*). The general folding is conserved in all class I cytochromes *c*, and structural studies and site-directed mutagenesis developed for mitochondrial or photosynthetic cytochrome models have been combined in an attempt to identify the essential residues necessary for electron transfer to take place (*7*, *8*). Despite considerable effort, no unique structural property has been established which controls the physicochemical characteristics of oxidoreduction and electron transfer in these molecules.

A recent structural comparison of a cytochrome involved in anaerobic metabolism with eukaryotic and prokaryotic cytochromes *c* has shown this molecule to be an interesting model for the study of the control of oxidoreduction potential in cytochromes (*9*, *10*). We have therefore focused our research on the cytochrome c_{553} isolated from the anaerobic bacteria, *Desulfovibrio*, to increase the knowledge of the structure−function relationships in the cytochrome *c* family.

Cytochrome c_{553} is a small cytochrome isolated from anaerobic bacteria involved in sulfate reduction. The oxidoreduction potential of this molecule is particularly low (40 mV) compared to those of mitochondrial or photosynthetic cytochromes (350−250 mV). Despite low sequence homology between cytochrome c_{553} and other cytochromes, interesting similarities have been found between the recently determined solution structure of this protein (*9*, *10*) and the structure of cytochrome *c* from aerobic organisms (*11*, *12*). The helical core is still present, and the hydrogen bonding network is similar to that found in tuna cytochrome *c*. The presence of an additional helix induces structural modifications around the axial methionine ligand. The major structural variation is an increase in heme accessibility in the molecule which may be responsible for the low oxidoreduction potential. Due to its unusual sequence, this cytochrome has been considered a natural variant of this class of molecules, permitting a better understanding of the structure−function relationship in the cytochrome *c* family.

Cytochrome c_{553} has been reported to interact with formate dehydrogenase. These molecules are both located in the periplasm of the same bacteria. This enzyme has been

* Corresponding author. Phone: 33 4 91 16 43 79. Fax: 33 4 91 16 45 78. E-mail: F.Guerlesquin@ibsm.cnrs-mrs.fr.
[‡] IBSM-CNRS.
[§] CEA-CNRS.

S0006-2960(98)00142-1 CCC: $15.00
Published on Web 05/19/1998

previously purified and characterized (*13*); it is a trimeric protein of 120 kDa comprising an α subunit of 83.5 kDa containing the molybdenum cofactor, probably involved in the catalytic process of formate oxidation, a β subunit of 27 kDa which contains the Fe−S centers, and a γ subunit of 14 kDa which holds a *c*-type heme.

We have undertaken cytochrome c_{553} engineering in an attempt to understand the electron transfer pathway from the electron donor center of formate dehydrogenase to the heme electron acceptor in cytochrome c_{553}. The interaction site between the two proteins has recently been investigated by site-directed mutagenesis. Mutation of the highly conserved K62 by a glutamic residue revealed the importance of electrostatic interactions between the two oxidoreduction partners (*14*). The Y64 residue located between the interacting site and the heme has been proposed to be involved in the electron transfer pathway. Previous biophysical studies of substituted Y64F, Y64L, Y64S, and Y64V mutants have demonstrated a modification of the dynamics of the molecule after Y64 replacement (*15*, *16*). In this work, we have carried out the Y64A substitution to determine if the aromatic ring is involved in electron exchange between formate dehydrogenase and cytochrome c_{553}. A conformational study of the Y64A mutant has been performed by NMR structure determination, and the functional effects of the substitution have been analyzed by kinetic measurements of electron exchange with formate dehydrogenase.

MATERIALS AND METHODS

Protein Purification. Desulfovibrio vulgaris Hildenborough cytochrome c_{553} was purified from *Desulfovibrio desulfuricans* G200 as previously reported (*17*), and formate dehydrogenase was prepared as previously described (*13*). Y64A cytochrome c_{553} was obtained by site-directed mutagenesis. A mutagenic oligonucleotide (5′GTCAAGAAAGCCTCTGATGAG3′) was designed to replace codon TAC encoding Y64 at positions 367−369 (Y) by codon GCC for alanine. The change was confirmed by dideoxynucleotide DNA sequencing. The *Hin*dIII−*Eco*RI fragment from the replicative form of the altered M13cyf was inserted into pJRD215, previously digested with the same two enzymes, to give pRC41Y64A. This recombinant plasmid was transformed into *Escherichia coli* DH5α cells and subsequently transferred to *D. desulfuricans* G200 as previously reported (*15*). The Y64A cytochrome c_{553} was purified from 350 g of wet cells of *D. desulfuricans* G200 (prc41Y64A) obtained from fermentation of 300 L of Postgate medium C supplemented with 0.28 mM kanamycin. The protein purification was the same as that for the wild-type protein (*17*).

Activity Assays. The activity assays were carried out by optical spectroscopy using the absorption at 553 nm of reduced cytochrome c_{553}, in the presence of 20 mM formate in 10 mM glycine/NaOH buffer at pH 8.3 and 25 °C. Formate dehydrogenase concentrations were 0.3, 0.6, and 3 nM, and the cytochrome c_{553} concentration ranged from 2 to 70 μM. The solution was incubated under an argon atmosphere for 15 min. To prevent oxygen oxidation, catalase (250 units/mL), glucose (25 mM), and glucose oxidase (0.5 unit/mL) were added to the solution. Optical measurements were carried out on a Beckman DU 7500 instrument.

^{1}H NMR Experiments. For NMR experiments, wild-type and Y64A cytochrome c_{553} were dissolved in 0.1 M potassium phosphate buffer (pH 5.9) containing 10% D_2O to a final concentration of 8 mM. Full reduction of the samples was obtained by addition of disodium dithionite in 0.1 M potassium phosphate at pH 8.0 under an argon atmosphere, at a final concentration of 30 mM. To avoid reoxidation of the ferrocytochrome, the NMR tubes were sealed under an argon atmosphere.

All NMR data were recorded at 310 K on a Bruker AMX-600 instrument operating at a proton frequency of 600 MHz equipped with a standard 5 mm Bruker probe with an internal B_0 gradient coil. Data were processed on Silicon Graphics workstations using Felix software provided by Molecular Simulation Inc. (MSI).

J-correlated spectra were obtained by TOCSY[1] experiments (*18*) and nOe-correlated spectra by NOESY experiments (*19*) in the phase sensitive mode with States−TPPI detection. These experiments were obtained under conditions previously described (*9*). NOESY experiments were collected with different mixing times of 50, 75, and 100 ms.

Computer-Aided Assignment. A computer-aided assignment was used for the assignment of distance restraints. The same protocol was performed in parallel for both the wild-type and the mutant cytochromes, to reduce the bias in the subsequent structure comparison. The assignment of the proton resonances was obtained using the Assign module of FELIX software, on the basis of the previously reported proton assignment for the wild-type cytochrome (*9*) and the previous manual assignment of the Y64A cytochrome. The nOe distance restraint calibration was performed using cross-relaxation volumes between atoms of known separation in rigid parts of the molecule. A factor of 20% was added to the resulting distance, to account for the inherent uncertainty in the distance calibration. Only upper bounds were used in the structure calculation. Assignment, restraint generation, and structure calculation were performed iteratively. Restraints that were violated, resulting from misassignment or overlapped peaks, were corrected after the first step of the calculation.

Structure Calculations. Structure calculations were performed using the DISCOVER program (MSI) interfaced to INSIGHTII for visualization and analytical purposes. The force field of AMBER4 was used as previously reported for ferrocytochrome c_{553} structure calculations (*10*). The different steps of the structure calculation were identical for the wild-type and the mutant cytochrome. The determination of a global fold was obtained by a simulated annealing (SA) protocol from randomized initial coordinates, as previously reported (*10*). Nine structures were obtained for both the wild-type and mutant cytochromes. A two-stage SA−restraint molecular dynamic (rMD) protocol was then applied to search the local conformation space available from the experimental constraints using the nine structures as initial coordinates. This two-step protocol is composed of a SA calculation using a simplified nonbonded term to facilitate

[1] Abbreviations: NOESY, nuclear Overhauser correlation spectroscopy; TOCSY, total correlation spectroscopy (by scalar coupling); SA, simulated annealing; rMD, restraint molecular dynamics; rmsd, root-mean-square deviation; Q_0, ubihydroquinone oxidase site; WT, wild-type.

exploration of conformational space and a high-temperature rMD refinement calculation using the AMBER4 force field with reduced charge and distance-dependent dielectric nonbonded interaction. The final minimized ensembles of 39 structures were used for structural analysis of both wild-type and mutant cytochromes. The coordinates of these 39 structures have been deposited in the Brookhaven Protein Data Bank (PDB code 2dvh).

Structure Analysis. An experimental violation function V_i was created and represented the sum of the energetic contributions from each distance constraint violated by more than 0.1 Å in the final minimized structure. The root-mean-square deviation (rmsd) of the structures was calculated over the specified atoms using INSIGHTII (MSI). The mean backbone structure was used for statistical characterization of the ensembles. The rmsds of the backbone dihedral angles from the ensemble means have been analyzed to give a quantitative measure of the backbone definition. The rmsd of the backbone conformation from the mean was calculated using the superimposition of backbone atoms from all residues and the deviation per residue calculated from this superimposition.

Hydrogen bonding analysis was performed with the 39 structures, using INSIGHTII. Two atoms were considered to form a hydrogen bond if the distance was less than 2.5 Å and the hydrogen bond angle was not less than 135°.

Electrostatic calculations were performed to give mean values over 12 randomly selected structures from each ensemble using Delphi as previously reported (*11*). Solvent accessibility calculations were performed using the Conolly algorithm as implemented in INSIGHTII.

RESULTS

Biochemical and Biophysical Characterization of Y64A Cytochrome c_{553}

Although *E. coli* can express cytochrome c_{553} in a functional form, the yield upon purification from cells was found to be much higher in a different *Desulfovibrio* strain (*D. desulfuricans* G200) (*17*). Y64A ferricytochrome c_{553} was isolated as previously reported for Y64F, -L, -S, and -V (*15*), with the same overproduction level in *D. desulfuricans* G200 as in other mutants (0.6 mg of pure protein per gram of cells). The mass spectrometry data (8830 Da) and the optical spectra ($\epsilon_{553} = 29\,500\ M^{-1}\ cm^{-1}$) were consistent with a mature cytochrome c_{553} production after the Y64A substitution. The redox potential (40 mV) was found to be almost unaffected by the mutation. On the other hand, the alkaline and acidic pK transitions of the axial methionine are notably affected; p$K_a = 2.7$ for Y64A instead of 1.9 for the wild-type protein, and p$K_b = 10.0$ for the mutant instead of 10.9 for the wild-type protein. These values observed for the Y64A mutant of *D. vulgaris* Hildenborough cytochrome c_{553} show however a high stability for the molecule, close to the properties of the wild-type cytochrome c_{553} from *D. desulfuricans* Norway (p$K_a = 2.8$ and p$K_b = 10.3$).

Aromatic flip rates have been previously used to compare the internal flexibility of the cytochrome c_{553} mutants (*15*); an increase of the internal flexibility is observed for Y64A (on Y7 and Y44, data not shown) as already reported for Y64L, -S, and -V mutants. Except for aromatic rings, the line width of most resonances in Y64A is comparable to that in the wild-type protein. Some other mutants (for instance Y64S) exhibit line broadening for backbone resonances; such a widespread broadening can be ascribed to chemical exchange processes between several conformations occurring at rates near the NMR time scale ($k \sim 10^2-10^3\ s^{-1}$). Partially denatured proteins (such as molten globules) usually exhibit broader resonances than tightly folded molecules (*20*). The lack of exchange broadening for Y64A can be interpreted as evidence for a deep minimum on the conformational energy surface, while other mutants correspond to flat energy surface. The similar spectral quality for both Y64A and the wild-type protein is a prerequisite for obtaining structural information with the same precision.

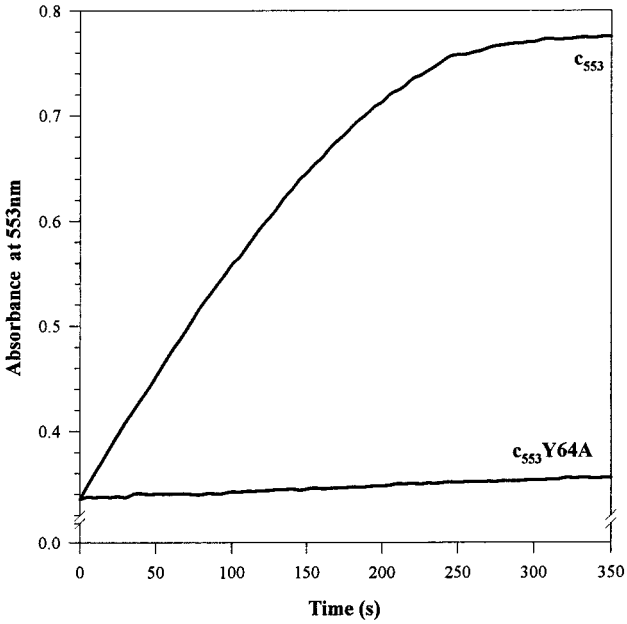

FIGURE 1: Time course of the reduction of cytochrome c_{553} from *D. vulgaris* Hildenborough and the Y64A mutant by formate dehydrogenase. The experiments were carried out using the absorption at 553 nm, in the presence of sodium formate, 0.3 nM formate dehydrogenase, and 26 μM cytochrome, at 25 °C. The buffer is 10 mM glycine/NaOH at pH 8.3 (optimal pH of the enzymatic activity).

Functional Properties of Y64A Cytochrome c_{553}

The functional effect induced by Y64A substitution was deduced from electron exchange measurements with the physiological partner, the formate dehydrogenase. Figure 1 presents the time course of the wild-type and Y64A cytochrome reduction in the presence of formate dehydrogenase. Study of the wild-type cytochrome c_{553} reduction by formate dehydrogenase has allowed us to determine the kinetic parameters of electron transfer within the complex. The initial reduction velocity for different wild-type cytochrome c_{553} concentrations (from 2 to 70 μM) was determined. From the sigmoidal curve, the Hill parameters ($k_{cat} = 111 \pm 2\ s^{-1}$ and $[S]_{0.5} = 5.3 \pm 1.8\ \mu M$) were established. The kinetics experiments performed with Y64A mutant cytochrome were inefficient whatever the cytochrome *c* concentration (2−70 μM) or formate dehydrogenase concentration (0.3−3 nM). The time course of reduction of Y64A cytochrome did not present a reduction process even after incubation for 12 h. We were unable to determine the kinetic constants of the complex involving the Y64A mutant.

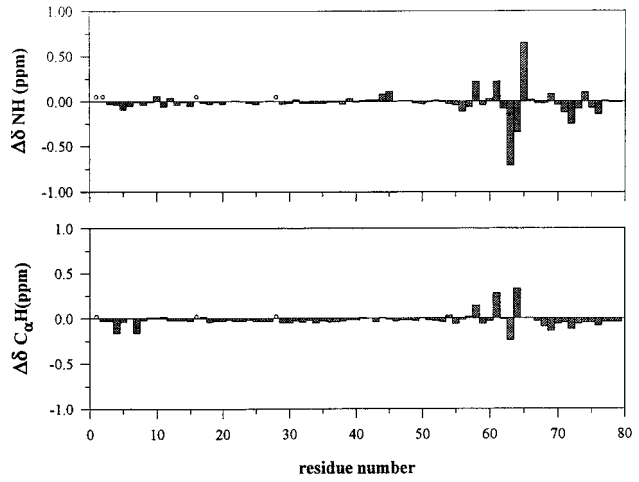

FIGURE 2: NH and C$^\alpha$H chemical shift variations induced by Y64A replacement.

The reduction of the other mutants (Y64F, Y64L, and Y64V) by formate dehydrogenase has also been studied. For Y64F cytochrome, the kinetic parameters ($k_{cat} = 35 \pm 5$ s^{-1} and $[S]_{0.5} = 12.4 \pm 3$ μM) were found to be significantly affected. But for Y64L and Y64V, the kinetic parameters were greatly modified and it was not possible to clearly establish the kinetic parameters from our experimental data.

NMR Chemical Shift Variations

Two-dimensional NMR is a useful method for comparing structural modifications in mutant cytochromes (*21*). We have compared the proton chemical shifts of the mutant and the wild-type ferrocytochromes c_{553}. Figure 2 illustrates the effect of Y64 substitution on the NH and C$^\alpha$H chemical shifts. We note that in the reduced state the chemical shift change occurs only in the vicinity of Y64 and affects the N- and C-terminal helices of the protein. From chemical shift variations, it was not possible to determine fine structural changes induced by the mutation, so on the basis of the NOESY experiments, we have measured distance restraints for the wild-type and mutant ferrocytochrome c_{553} to elucidate the three-dimensional structure modifications induced by the mutation.

Structure Determination

Using the computer-aided assignment from the module Assign from Felix software, we have quantified 767 restraints for the wild-type protein and 807 for the Y64A mutant. These restraints were used to generate structural models for both molecules. The restraint variations between native and mutant cytochrome c_{553} are presented in Figure 3. The nOe distribution is equivalent for both molecules except for Y7 which is better resolved in the mutant protein spectra and Y64 which has a long side chain compared to A64. The backbone coordinates of the 39 structures calculated for the wild-type cytochrome and for the Y64A mutant were obtained from a protocol previously developed for the ferrocytochrome c_{553} structure elucidation (*10*).

Structure Analysis

The backbone rmsd of the whole ensemble of 39 structures was 0.83 (±0.12) Å for the native protein and 0.77 (±0.12) Å for the mutant. Analysis of the two ensembles is given in Table 1. For the two proteins, the secondary structure elements, in particular the four helices, are similarly well defined. The ensemble of secondary structural motifs is identical to that described by Blackledge et al. (*10*) for the wild-type protein. The two molecules are composed of four helices: helix 1 for the N-terminal helix (residues 4−14), helix 2 for residues 35−46, helix 3 for the methionine ligand-containing helix (residues 55−61), and helix 4 for the C-terminal helix (residues 67−79). Helix 1, helix 2, and helix 4 are preserved in the vast majority of the cytochrome *c*, as well as the Ω-loop comprising residues 17−28.

Local Backbone Variation. The conformational dispersion of the ensemble for wild-type and Y64A mutant cytochromes is illustrated by the rmsd of the backbone atomic coordinates for the 39 structures in comparison to the mean structure (Figure 4A,B). For both proteins, the same regions of local disorder were observed at residues 47−54 and the middle section of the Ω-loop (residues G24−S25), as previously reported (*10*). At position 64, the backbone rmsd value is correlated to a well-defined structure for the long side chain of tyrosine and a less well-defined structure of the short side chain for alanine.

The superimposition of the backbone coordinates for the two mean structures is shown in Figure 5. The backbone deviation between the mean structures from the two proteins is 0.91 and 1.25 Å for heavy atoms, with significant variations in the vicinity of residues G24 and G31. In both cases, it is impossible to solve the real structural difference between wild-type and mutant protein, due to the reduced structural information available from glycine residues (no side chain and, in our case, no stereospecific assignment of the C$^\alpha$ protons) that leads to regions that are poorly determined by the structure calculations.

No significant difference between the Ψ dihedral angle mean values is observed between the two proteins. Standard deviations reproduce the observations noted for the backbone rmsd. The same analysis can be performed for Φ dihedral angle values (data not shown).

Hydrogen Bonding Networks. The hydrogen bonding networks present in the ensemble of structures for both proteins are shown in the two-dimensional plot in Figure 6. The plot identifies the presence of hydrogen bonds between two residues in more than 25% of the structures. The ensemble of hydrogen bonds was similar for mutant and wild-type proteins and has been described previously for the wild-type cytochrome (*10*). Nevertheless, the few differences are worth noting. (1) In the wild-type protein, Y64 forms hydrogen bonds with L6 and S9. The absence of the Y64 side chain in the Y64A mutant decreases the number of hydrogen bonds but does not appear to create structural variations or new hydrogen bonding (Figure 7A). The absence of hydrogen bonds with the N-terminal helix in the mutant is probably the cause of the protein destabilization observed through the acidic and basic p*K* transition measurement and the chemical shift variations observed at the N- and C-terminal helices. Moreover, the absence of these hydrogen bonds probably has an effect on the ring mobility of Y7, as previously reported. (2) The mutation also induces a loss of hydrogen bonds in the heme pocket (Figure 7B). In wild-type cytochrome c_{553}, hydrogen bonds are observed between the heme and residues S25, K27, Q32, K40, Y44,

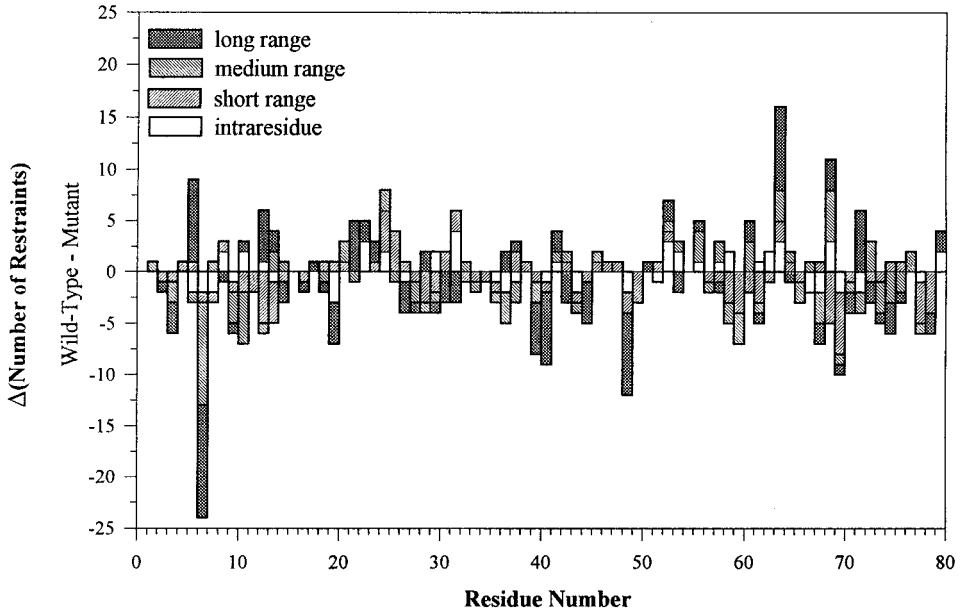

FIGURE 3: Difference in the distance restraints obtained for the wild type and the mutant ferrocytochrome c_{553}. The number of distance restraints per residue used for the structure calculations of wild-type and Y64A cytochrome c_{553} is as follows: long-range distances between residues i and $i + n$ ($n > 4$), 194 for the wild type and 206 for the mutant; medium-range distances for residues i and $i + n$ ($1 < n < 5$), 150 and 163 for the WT and the Y64A mutant, respectively; and short-range distances for residues i and $i + 1$, 216 for the WT and 237 for the mutant. Residue 80 is the heme moiety.

Table 1

	wild type	Y64A
Energetic Statistics[a]		
bond	12.85 ± 0.63	13.71 ± 0.60
angle	91.87 ± 6.75	100.76 ± 5.19
dihedral	79.56 ± 5.8	87.00 ± 5.35
out of plane	2.84 ± 0.63	3.26 ± 0.68
H bond	−35.38 ± 1.58	−35.82 ± 1.93
VDW	−248.51 ± 7.69	−244.12 ± 6.31
electric static	−1009.17 ± 15.75	−959.28 ± 16.28
total	−1104.82 ± 20.46	−1033.43 ± 18.26
Experimental Statistics		
no. of distance violations		
>0.1 Å	18.36 ± 4.27	24.64 ± 3.98
>0.2 Å	3.15 ± 1.58	7.02 ± 1.75
>0.3 Å	0.31 ± 0.52	1.20 ± 1.03
violation energy (>0.1 Å)	16.25 ± 3.92	25.41 ± 3.34
Structural Statistics		
backbone atom[b] (residues 1−79) rmsd to mean[c]	0.83 ± 0.12	0.77 ± 0.12
heavy atom (residues 1−79) rmsd to mean	1.23 ± 0.12	1.20 ± 0.17
backbone atom (residues 3−77) rmsd to mean	0.69 ± 0.08	0.68 ± 0.12
heavy atom (residues 3−77) rmsd to mean	1.17 ± 0.11	1.17 ± 0.18

[a] All values are in kilocalories per mole. [b] Backbone atoms used for superposition are N, C^{α}, and C. [c] rmsd values are the average pairwise rmsd for the residue and atoms shown.

Y49, and K54 (Table 2). The differences observed at the heme cleft between K54 and the Ω-loop (S25) are located in this flexible region of the molecule. It is difficult to determine whether these variations in hydrogen bonding network correspond to real structural changes or just to a variation in statistical repartition of the hydrogen bond in the different structures. The absence of hydrogen bonds with Y44 could explain the increase in the internal mobility found in the mutants.

Electrostatic Distribution and Heme Solvent Accessibility. The ionic strength dependence of the complex formation between cytochrome c_{553} and formate dehydrogenase has recently been demonstrated (*14*). Y64 is situated in the region of the proposed encounter surface of the protein (*11*), and its substitution may induce electrostatic or solvent accessibility changes. The heme exposure is shown for the two NMR ensembles in Figure 8A. This clearly demonstrates that in the absence of the aromatic ring there is an increase in heme solvent accessibility at the C10 edge. The

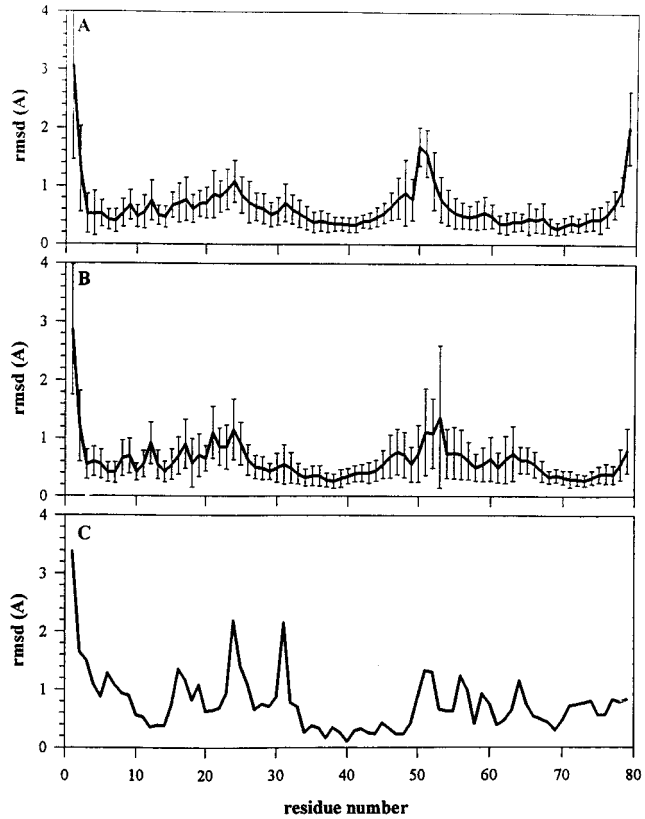

FIGURE 4: Positional backbone rmsd and variance for (A) wild-type cytochrome c_{553}, (B) Y64A cytochrome c_{553}, and (C) both.

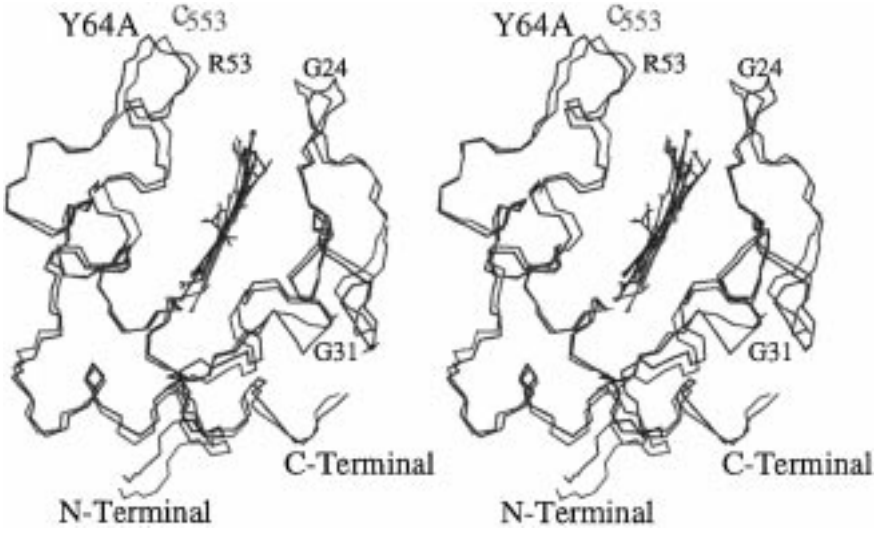

FIGURE 5: Stereoview of the superimposition of the backbone coordinates of the representative structures of the wild-type (red) and Y64A (blue) cytochrome c_{553}.

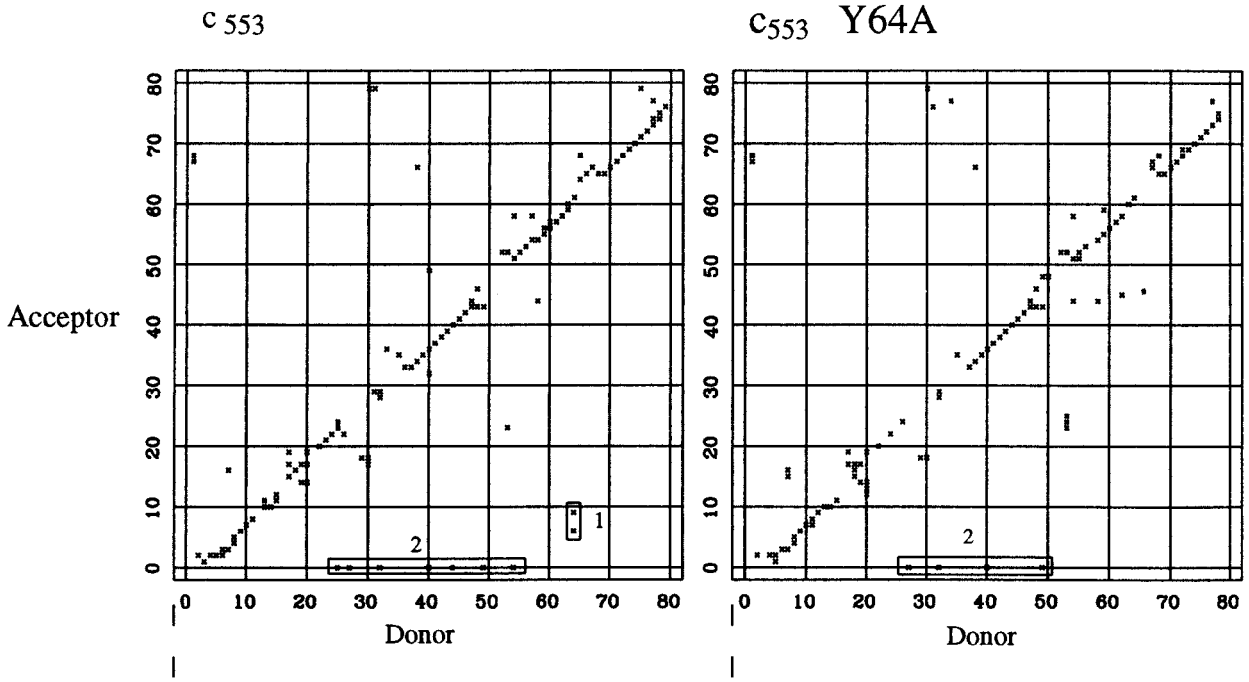

FIGURE 6: Matrix representation of the hydrogen bonding networks in wild-type and Y64A ferrocytochrome c_{553}. The numbers refer to the discussion of the hydrogen bonding networks identified in the text. Only those hydrogen bonds occurring in more than 10 of the 39 structures are shown. The heme is indicated as residue 0.

increased accessibility appears to be due not only to the absence of the aromatic side chain but also to the increased disorder present in the ensemble for the side chain of K63. This also affects the mean electrostatic surface shown in Figure 8B, resulting in a more diffuse positive charge above the cysteine edge.

Cavity Induced by Y64A Substitution. Y64 is contained in a large turn region which forms an important hydrophobic pocket in the interior of the molecule. This aromatic residue makes a linkage between the heme and the encounter surface. Tyrosine replacement by a phenylalanine residue removes the hydrogen bond between the tyrosine hydroxide and S9 HG and L6 CO. The ring substitution in the case of Y64L, -V, and -A mutants affects the hydrophobic heme environment progressively. Moreover, the Y64A substitution increases the size of the cavity adjacent to the position of residue 64 (Figure 8B). It should be noted that, in the case of *D. desulfuricans* Norway cytochrome c_{553} (*22*), Y64 is replaced by a leucine residue and S9 is replaced by a methionine residue. The methionine residue might offer a compensatory effect for Y64L replacement in obtaining an overall packing and hydrophobicity in the pocket between residues 6 and 64.

DISCUSSION

The physical basis of electron transfer in oxidoreduction complexes is a subject of considerable debate. Two mechanisms have been proposed, incorporating through-bond and through-space pathways. The through-space path is probably the least efficient because of the exponential decay of the interaction with distance. The covalently bonded path can be extremely long compared to the direct through-space path,

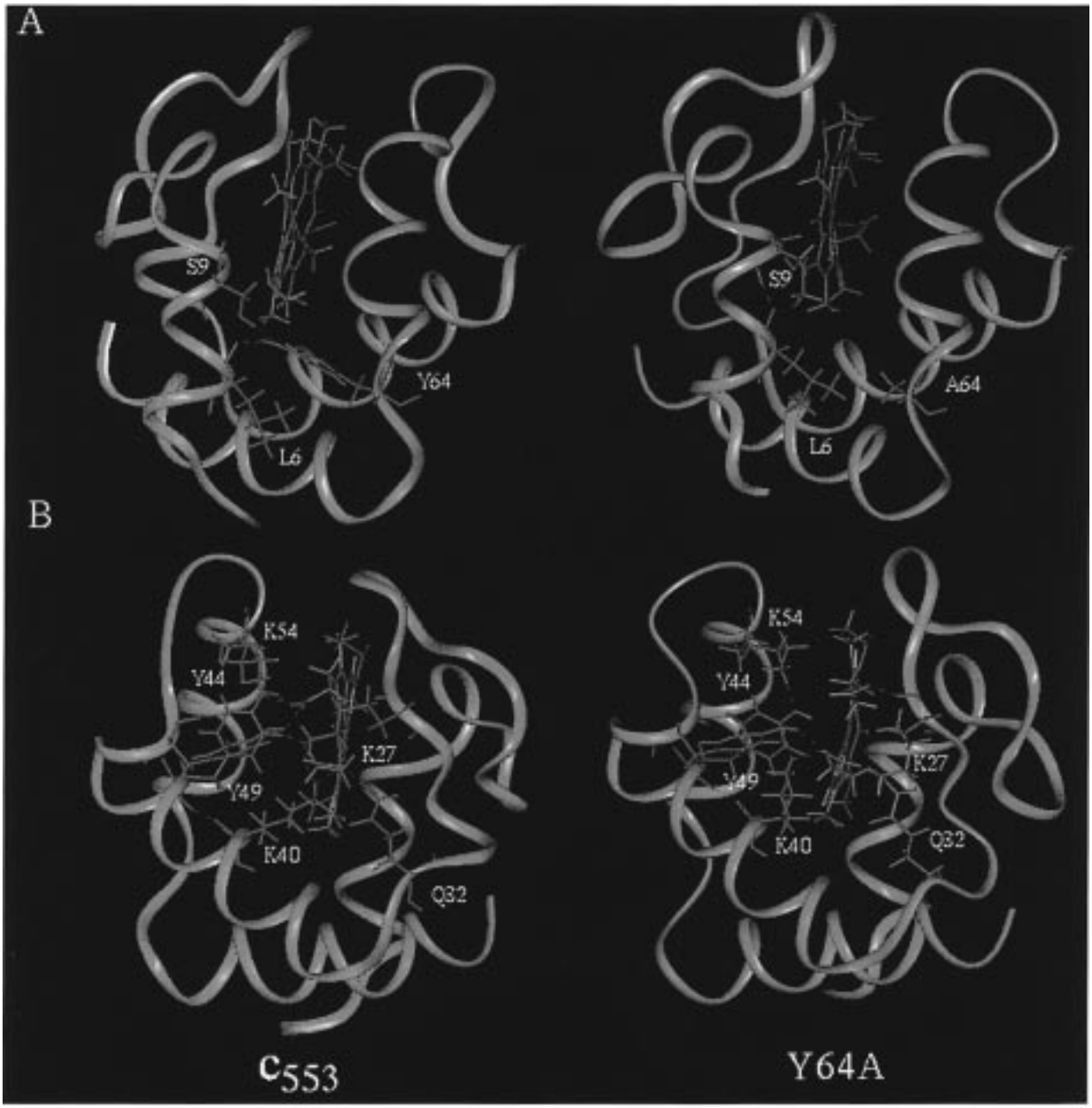

FIGURE 7: Hydrogen bonding networks. Hydrogen bonds are noted by broken lines. Representation of hydrogen bonds (A) with residue 64 and (B) in the heme pocket (left) for the wild-type cytochrome c_{553} and (right) for the Y64A mutant.

Table 2: Heme Pocket and Related Hydrogen Bonds

donor	group	acceptor	group	WT	Y64A
Ser25	HG	heme	OC	7/39	0/39
Lys27	NH	heme	OC	27/39	38/39
Lys27	HN3	heme	OC	18/39	13/39
Lys27	HN3	heme	OD	34/39	17/39
Gln32	HE*	heme	HD	37/39	34/39
Lys40	HN3	heme	OD	39/39	25/39
Tyr44	HH	heme	OC	18/39	0/39
Tyr49	HH	heme	OC	4/39	11/39
Tyr49	HH	heme	OD	26/39	30/39
Lys54	HN3	heme	OC	13/39	7/39

but in this case, the electron transfer rates depend on the number of covalent bonds separating the donor and the acceptor rather than on the direct separation distance. The through-bond pathway involves different mechanisms: (i) direct coupling of metal and ligands (in this case, the electron is considered completely delocalized), (ii) covalent σ-bonded bridges which connect the donor and acceptor (1.5 Å), and (iii) nonbonded exchange which associates donor and acceptor in an interaction through nonbonded groups. Several groups have investigated potential electron transfer pathways in proteins, although the identification of a unique through-bond pathway is complicated by the large number of possible combinations. It is therefore very important to identify residues which can be shown to participate in the electron transfer process and, if possible, to establish the physicochemical properties necessary at a given point in the electron transfer pathway.

In this work, we have demonstrated the functional role of Y64 in *D. vulgaris* Hildenborough cytochrome c_{553}; the substitution was drastic for the electron exchange between cytochrome c_{553} and the formate dehydrogenase but does not affect the oxidoreduction potential or the stability of the

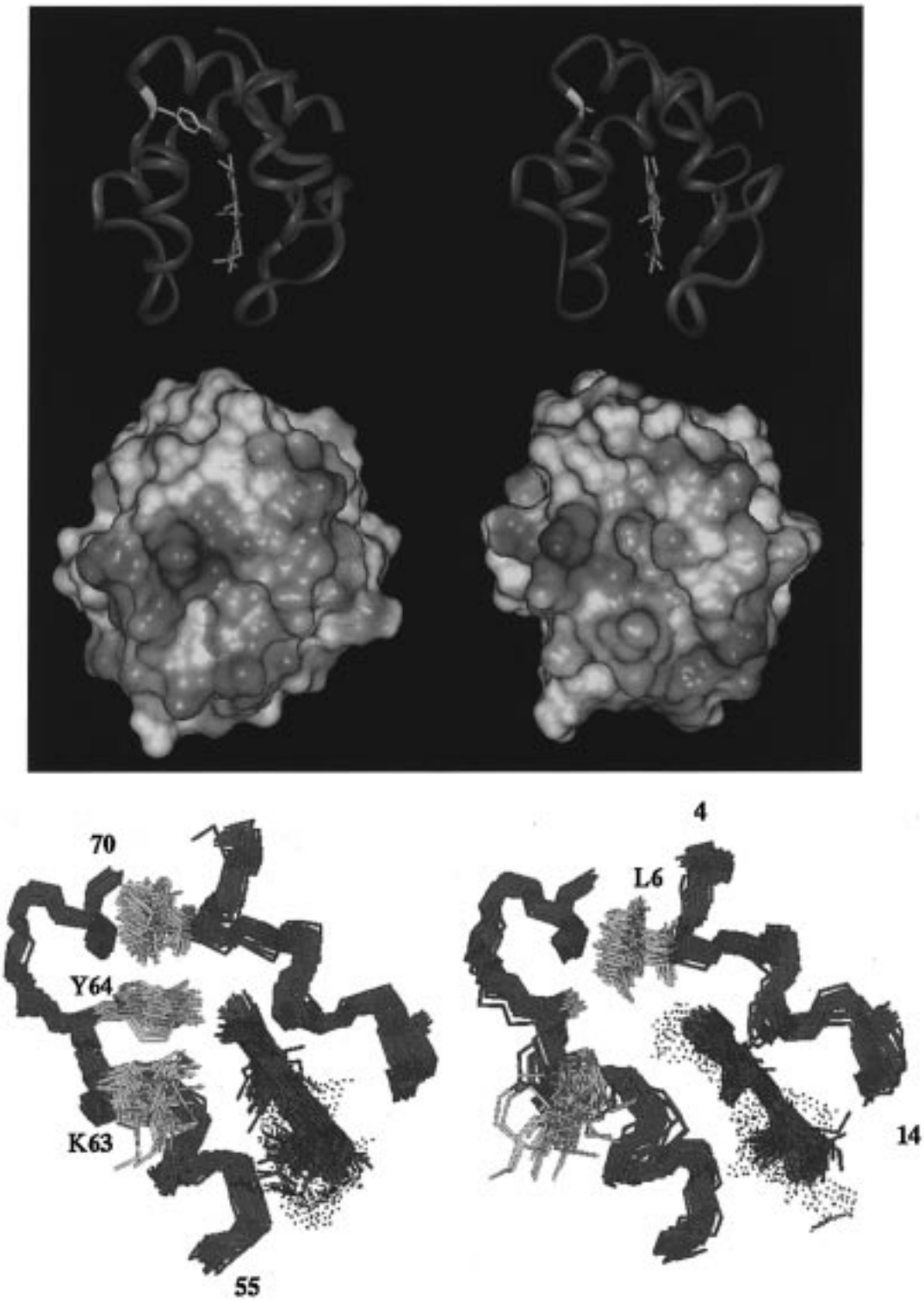

FIGURE 8: (A, top two pairs of structures) Electrostatic charge distribution of the encounter surface of wild-type (left) and Y64A (right) ferrocytochrome c_{553}. The mean values is taken for 12 randomly selected structures from the two ensembles. The values of the electrostatic grids are shown at the surface of the molecule, calculated using the Conolly algorithm for the closest structure to the mean of the two ensembles. The heme solvent accessibility is shown in orange. The remaining color sheme for the surfaces is scaled from −3 kT for red, through white, to blue for 3 kT. The ribbon is shown above each molecule in the same orientation. (B, bottom) Heme pocket architecture of NMR ensembles of wild-type (left) and Y64A (right) cytochrome c_{553}. The backbones of residues 4−14 and 55−70 are shown in blue and the heavy atoms of residues 6, 63, and 64 in yellow, and the heme is shown in red. The accessibility of the heme of the structure closest to the mean of each ensemble is shown in black.

protein. Kinetic studies of Y64F, Y64L, and Y64V mutants provide evidence that the substitution decreases drastically the electron exchange. The Y64A mutant was not reduced after incubation for 12 h with the redox partner. It appears therefore that substitution of the Y64 with alanine has induced either an inhibition of complex formation or a loss of the electron transfer pathway within the complex. We have undertaken the structure determination of the Y64A mutant to investigate these possibilities. From the two-dimensional (2D) ^{1}H NMR study, we could solve the

structure of both the wild-type and Y64A ferrocytochromes c_{553} with the same protocol. The NMR spectral quality and chemical shift variations were consistent with a highly conserved structure for both the wild-type and mutant proteins. The structural analysis of the mutant protein demonstrates that in general the structure of the wild type is highly conserved in the Y64A mutant and that the electrostatic charge at the surface is conserved and the hydrogen bonding network virtually unaffected. The major differences between the two molecules are in the heme−solvent interface, a region already implicated in the electron transfer process involving cytochromes *c* (*5*, *11*). Two significant effects are observed: an increase in the accessibility of the cysteine edge of the heme and a redistribution of the mean charge at the surface of the molecule. The former effect appears to be due both to the increased disorder of the surface K63 and to the absence of Y64. The reason for this increased disorder is possibly the rupture of the cation−π interaction (*23*) between the charged side chain and the aromatic ring. Although this interaction is not observed throughout the wild-type ensemble, possibly due to the absence of this type of attraction in the rMD force field, the proximity of the two side chains suggests the existence of a cation−π bond between Y64 and K63. The consequent reorientation of the K63 side chain modifies slightly the cluster of positive charges around the heme pocket. We have already reported that the substitutions K62E and K62E/K63E affect the association constant of the complex formation by factors of 3 and 5, respectively (*14*), but do not inhibit the electron transfer between formate dehydrogenase and cytochrome *c*. Consequently, in the case of Y64A substitution, the reorientation of K63 is not sufficient to explain the loss of electron transfer between the two partners. We conclude that Y64 is required for the electron transfer pathway.

Different authors have developed site-directed mutagenesis studies of cytochrome *c* in which aromatic residues were supposed to be involved in the electron pathway. Phe82 in mitochondrial cytochromes is structurally equivalent to Y64 in cytochrome c_{553} (*11*). The kinetic measurements of electron exchange between yeast cytochrome and Zn-substituted cytochrome *c* peroxidase have been carried out for five mutants (F82Y, -G, -S, -L, and -I) (*24*). The authors reported that, for four variants with an aliphatic residue at position 82, the rate of electron exchange was 10^4 times slower at 0 °C than for the two molecules with aromatic residues. However, the midpoint potentials were also significantly affected by the substitution. Structural studies by either 2D NMR (F82Y) (*25*) or X-ray crystallography (F82S and -G) (*26*, *27*) reveal some conformational variations. From the study of F82 variants, it was suggested that F82 has at least three roles: (i) limiting solvent accessibility to the heme, thereby regulating the reduction potential of the protein, (ii) facilitating the rate of electron transfer by providing the optimal medium along the electron pathway, and (iii) forming a contact face interaction with the redox partners to assist in the formation of the productive electron transfer complex.

Y67 involvement in electron transfer in mitochondrial cytochromes was also studied with site-directed mutagenesis (*7*). Conversion of Y67F results in a substantial increase in the size of an already existing internal cavity adjacent to residue 67. The involvement of this residue in the stabilization of oxidoreduction states through a hydrogen bond network involving a structural water molecule was proposed by the authors (*28*). However, the modification of the oxidoreduction potential induced by the mutation is 50 mV, suggesting a second role for Y67 in setting the value of the midpoint reduction potential.

Evidence of the role of an aromatic residue in electron transfer has been obtained in the cytochrome *b* subunit of the cytochrome bc_1 complex. Y147 is a highly conserved residue; Y147F and -V replacements significantly affect the electron transfer between the ubihydroquinone oxidase (Q_0) site and the cytochrome *b*, and the electron exchange was found to be dramatically altered in Y147A and -S mutants. These mutations affect the electron exchange but do not change the oxidoreduction potential of the redox centers and do not modify either their accessibility or the substrate binding site (*29*). Two pseudorevertants at the highly conserved M154 position (M154I and -V) were found to restore the electron exchange rates from the Q_0 site to the cytochrome *b*. The compensatory effects of M154 substitutions were only needed when position 147 is occupied by a small amino acid side chain (A or S). These spatial interactions between positions 147 and 154 suggest that to be efficient, electron transfer requires either a bulky side chain at position 147 or a hydrophobic side chain at position 154 when the former residue is occupied with small residues. This result is consistent with our data on *Desulfovibrio* cytochromes c_{553}, indicating that the electron exchange takes place only if some important amino acid side chains form hydrogen bonds to allow a through-bond pathway.

Our results clearly show that the difference in kinetics rates between Y64 and F64 cytochromes c_{553} is correlated with the loss of a hydrogen bond involving the hydroxide group of the tyrosine and L6 and S9 residues. The replacement of Y64 by L, V, or A increases the distance between the amino acid side chain of the substitute residue and both the L6 and S9 side chains. *D. desulfuricans* Norway cytochrome c_{553} may be considered a natural revertant of the Y64L mutant where the S9 side chain is substituted by the M9 side chain, producing an active cytochrome. The next step of our study will be either to determine the structure of this natural revertant or to make a double S9M/Y64L mutant of *D. vulgaris* Hildenborough cytochrome to check the involvement of these two residues in the electron transfer pathway. Many groups have attempted to provide direct experimental evidence of electronic coupling mediated by hydrogen bonds (*30*, *31*). On the basis of these results, we have studied the electron pathway within cytochrome c_{553}, using the Greenpath software (*32*). From Y64 to the heme iron, four residues are proposed to be involved in a through-bond electron transfer (L6, Y7, C10, and H14). After Y64F, -L, -S, and -V substitutions, the through-bond electron path is forced to become a less efficient through-space electron path. In the case of Y64A replacement, the through-space electron transfer becomes unproductive. Our results demonstrate that *D. vulgaris* Hildenborough cytochrome c_{553} is an excellent candidate for evaluating this electronic coupling in cytochromes *c*, and further investigation using protein engineering will be undertaken to elucidate the different intermediates of the through-bond electron path in cytochromes *c*.

ACKNOWLEDGMENT

Dr. J. D. Wall is kindly thanked for the conjugational gene transfer from *E. coli* to *D. desulfuricans* G200 and Dr. L. Blanchard for the helpful discussion.

SUPPORTING INFORMATION AVAILABLE

Proton chemical shifts of Y64A cytochrome c_{553} at 37 °C (1 page). Ordering information is given on any current masthead page.

REFERENCES

1. Bertrand, P. (1991) in *Structure Bonding: Long-Range Electron Transfer in Biology*, pp 3−47, Springer-Verlag, Berlin.
2. Kuki, A. (1991) in *Structure Bonding: Long-Range Electron Transfer in Biology*, pp 50−83, Springer-Verlag, Berlin.
3. Tsukihara, T., Aoyama, H., Yamashita, E., Tomizaki, T., Yamaguchi, H., Shinzawa-Itoh, K., Nakashima, R., Yaono, R., and Yoshikawa, S. (1996) *Science 272*, 1136−1144.
4. Deisenhofer, J., Epp, O., Miki, K., Huber, R., and Michel, H. (1985) *Nature 318*, 618−629.
5. Moore, G., and Pettigrew, G. (1990) in *Cytochromes c: Evolutionnary, Structural and Physiological Aspects*, Springer-Verlag, Berlin.
6. Mauk, A. G (1991) *Struct. Bonding (Berlin)*, 131−157.
7. Berghuis, A. M., Guillemette, J. G., Smith, M., and Brayer G. D. (1994) *J. Mol. Biol. 235*, 1326−1341.
8. Caffrey, M. S. (1994) *Biochimie 76*, 622−630.
9. Marion, D., and Guerlesquin, F. (1992) *Biochemistry 31*, 8171.
10. Blackledge, M., Medvedeva, S., Poncin, M., Guerlesquin, F., Bruschi, M., and Marion, D. (1995) *J. Mol. Biol. 245*, 661−681.
11. Blackledge, M., Guerlesquin, F., and Marion, D. (1995) *Proteins 24*, 178−194.
12. Blackledge, M., Guerlesquin, F., and Marion, D. (1995) *Nat. Struct. Biol. 2*, 532−535.
13. Sebban, C., Blanchard, L., Bruschi, M., and Guerlesquin, F. (1995) *FEMS Microbiol. Lett. 133*, 143−149.
14. Sebban-Kreuzer, C., Dolla, A., and Guerlesquin, F. (1998) *Eur. J. Biochem.* (in press).
15. Blanchard, L., Dolla, A., Marion, D., Bersch, B., Forest, E., Bianco, P., Wall, J., and Guerlesquin, F. (1994) *Eur. J. Biochem. 226*, 423−432.
16. Sebban-Kreuzer, C., Blanchard, L., Bersch, B., Blackledge, M., Marion, D., Dolla, A., and Guerlesquin, F. (1998) *Eur. J. Biochem. 251*, 787−794.
17. Blanchard, L., Marion, D., Pollock, B., Voordouw, G., Wall, J., Bruschi, M., and Guerlesquin, F. (1993) *Eur. J. Biochem. 218*, 293−301.
18. Davis, D. G., and Bax, A. (1985) *J. Am. Chem. Soc. 107*, 2820−2821.
19. Macura, S., Huang, Y., Suter, D., and Ernst, R. R. (1981) *J. Magn. Reson. 43*, 259−281.
20. van Dael, H., Haezebrouck, P., Morozova, L., Arico-Muendel, C., and Dobson, C. M. (1993) *Biochemistry 32*, 11886−11894.
21. Pielak, G. J., Atkinson, R. A., Boyd, J., and Williams, J. P. (1988) *Eur. J. Biochem. 177*, 179−185.
22. Bruschi, M., Woudstra, M., Campese, D., and Bonicel, J. (1993) *Biochim. Biophys. Acta 1162*, 89−92.
23. Dougherty, D. A. (1996) *Science 271*, 163−168.
24. Liang, N., Mauk, A. G., Pielak, G. J., Johnson, J., Smith, M., and Hoffman, B. M. (1988) *Science 240*, 311.
25. Pielak, G. J., Atkinson, R. A., Boyd, J., and Williams, R. J. P. (1988) *Eur. J. Biochem. 177*, 179−185.
26. Louie, G. V., Pielak, G. J., Smith, M., and Brayer, G. D. (1988) *Biochemistry 27*, 7870−7876.
27. Louie, G. V., and Brayer, G. D. (1989) *J. Mol. Biol. 209*, 313−322.
28. Berghuis, A. M., and Brayer, G. D. (1992) *J. Mol. Biol. 223*, 959−976.
29. Saribas, A. S., Ding, H., Dutton, P. L., and Daldal, F. (1995) *Biochemistry 34*, 16004−16012.
30. de Rege, P. J. F., Williams, S. A., and Therien, M. J. (1995) *Science 269*, 1409−1412.
31. Wuttke, D. S., Bjerrum, M. J., Winkler, J. R., and Gray, H. B. (1992) *Science 256*, 1007−1009.
32. Regan, J. J., Risser, S. M., Beratan, D. N., and Onuchic, J. N. (1993) *J. Phys. Chem. 97*, 13083−13088.

BI980142U